Journal of Archaeological Science 157 (2023) 105827

Contents lists available at ScienceDirect

Journal of Archaeological Science

journal homepage: www.elsevier.com/locate/jas

An arrowhead made of meteoritic iron from the late Bronze Age settlement of Mörigen, Switzerland and its possible source

Beda A. Hofmann [a,b,*], Sabine Bolliger Schreyer [c], Sayani Biswas [d], Lars Gerchow [d], Daniel Wiebe [e], Marc Schumann [e], Sebastian Lindemann [e], Diego Ramírez García [e], Pierre Lanari [b], Frank Gfeller [a,b], Carlos Vigo [d], Debarchan Das [d], Fabian Hotz [d], Katharina von Schoeler [f,d], Kazuhiko Ninomiya [g], Megumi Niikura [h], Narongrit Ritjoho [i], Alex Amato [d]

[a] *Naturhistorisches Museum Bern, Bernastrasse 15, CH-3005, Bern, Switzerland*
[b] *Institute of Geological Sciences, University of Bern, Baltzerstrasse 1+3, CH-3012, Bern, Switzerland*
[c] *Bernisches Historisches Museum, Helvetiaplatz 5, CH-3005, Bern, Switzerland*
[d] *Paul Scherrer Institute, Forschungsstrasse 111, CH-5232, Villigen PSI, Switzerland*
[e] *Physics Insitute, University of Freiburg, Hermann-Herder-Strasse 3, D-79104, Freiburg, Germany*
[f] *Institute for Particle Physics and Astrophysics, ETH Zürich, 8093, Zürich, Switzerland*
[g] *Institute of Radiation Sciences, Osaka University, Toyonaka, Osaka, Japan*
[h] *RIKEN Nishina Center for Accelerator Based Science, Hirosawa 2-1, Wako, 351-0198, Saitama, Japan*
[i] *School of Physics, Institute of Science, Suranaree University of Technology, 111 University Avenue Muang, Nakhon Ratchasima, 30000, Thailand*

A R T I C L E I N F O

Keywords:
Arrowhead
Meteoritic iron
Bronze Age
Muon induced X-ray emission (MIXE)
Gamma spectrometry
X-ray fluorescence spectrometry
Switzerland

A B S T R A C T

A search for artefacts made of meteoritic iron has been performed in archaeological collections in the greater area of the Lake of Biel, Switzerland. A single object made of meteoritic iron has been identified, an arrowhead with a mass of 2.9 g found in the 19th Century in the late Bronze Age (900–800 BCE) lake dwelling of Mörigen, Switzerland. The meteoritic origin is definitely proven by combining methods extended and newly applied to an archaeological artefact. Elemental composition (7.10–8.28 wt% Ni, 0.58–0.86 wt% Co, ~300 ppm Ge), primary mineralogy consisting of the associated Ni-poor and Ni-rich iron phases kamacite (6.7 wt% Ni) and taenite (33.3 wt% Ni), and the presence of cosmogenic ^{26}Al ($1.7^{+0.5}_{-0.4}$ dpm/kg). The Ni-rich composition below the oxidized crust and the marked difference to meteorites from the nearby (4–8 km) Twannberg iron meteorite strewn field is confirmed by muon induced X-ray emission spectrometry (8.28 wt% Ni). The Ni-Ge-concentrations are consistent with IAB iron meteorites, but not with the Twannberg meteorite (4.5 wt% Ni, 49 ppm Ge). The measured activity of ^{26}Al indicates derivation from an iron meteorite with a large (2 t minimum) pre-atmospheric mass. The flat arrowhead shows a laminated texture most likely representing a deformed Widmanstätten pattern, grinding marks on the surface and remnants of wood-tar. Among just three large European IAB iron meteorites with fitting chemical composition, the Kaalijarv meteorite (Estonia) is the most likely source because this large crater-forming fall event happened at ~1500 years BC during the Bronze Age and produced many small fragments. The discovery and subsequent transport/trade of such small iron fragments appears much more likely than in case of buried large meteorite masses. Additional artefacts of the same origin may be present in archaeological collections.

1. Introduction

Metallic iron was available to humans in the form of rare meteoritic iron before the smelting of the metal from oxide ores started. The use of meteoritic iron for the fabrication of objects in pre-Iron Age times in Eurasia and northern Africa is known from find complexes in Turkey, Greece, Syria, Iraq, Lebanon, Egypt, Iran, Russia and China (Rickard 1941; Shramko et al., 1965; Shramko 1981; Bjorkman 1973; Buchwald

* Corresponding author. Naturhistorisches Museum Bern, Bernastrasse 15, CH-3005, Bern, Switzerland.
E-mail address: beda.hofmann@geo.unibe.ch (B.A. Hofmann).

https://doi.org/10.1016/j.jas.2023.105827
Received 6 March 2023; Received in revised form 4 July 2023; Accepted 14 July 2023
Available online 25 July 2023
0305-4403/

2005; Johnson et al., 2013; Rehren et al., 2013; Comelli et al., 2016; Johnson and Tyldesley 2016; Matsui et al., 2022; Ströbele et al., 2016; Broschat et al., 2018; Chen et al., 2018; Jambon and Doumet-Serhal, 2018; Zavyalov and Terekhova, 2019; see Supplementary materials Table S1). Finds of meteoritic iron artefacts in central and western Europe are very rare and up to now restricted to two sites in Poland: The two Czestochowa-Rakowa bracelets (Jambon 2017; Kotowiecki 2004; Piaskowski 1982) and the Wietrzno axe (Kotowiecki 2004; Jambon 2017). In total, only 21 find complexes (not all verified with modern methods) comprising a maximum of 54 individual objects of pre-Iron Age meteoritic artefacts were previously known from Eurasia and northern Africa (Table S1). In other parts of the world, the use of meteoritic iron is of younger date, starting ~2000 years ago in North America (McCoy et al., 2017) while the spread of meteoritic iron from the Cape York meteorite in Greenland and to Canada dates back to ~800 CE (Buchwald 2005). Searches for meteoritic iron in archaeological collections have been performed by Jambon (2017) and Tamm (2014), without revealing unknown objects of meteoritic origin. As part of this study, archaeological collections in Switzerland with many objects from the area of Lake of Biel were investigated using a portable X-ray fluorescence (pXRF) analyzer. The aim was to identify potential objects made of meteoritic iron from the nearby Twannberg iron meteorite strewn field.

While no object made of the Twannberg iron meteorite was identified during this study, we report the identification of an arrowhead made of a clearly different iron meteorite. This specimen was found in a late Bronze Age pile-dwelling site at Mörigen, Lake of Biel, Switzerland (47° 5.20′N 7° 12.13′E, center of excavation site). The late Bronze Age date (900–800 BCE) is based on typology of associated ceramics and bronze artefacts (Bernatzky-Götze 1987). Mörigen is located just 4–8 km southwest of the large Twannberg iron meteorite strewn field with more than 2000 individual finds totalling ~150 kg (Hofmann et al., 2009; Smith et al., 2017). The Mörigen pile dwelling was known since 1843, first sampled by fishermen and excavated 1873/74 (von Fellenberg, 1875; Ischer 1911; Tschumi 1953).

While previous analyses of archaeological objects made of meteoritic iron either used destructive/invasive methods and/or X-ray fluorescence (XRF) and scanning electron microscopy-energy dispersive spectroscopy (SEM-EDS) techniques, we relied on a combination of several exclusively non-destructive methods including previously used XRF (with a new calibration for Ge and Ga) and SEM-EDS, extended with muon induced X-ray emission spectrometry (MIXE) and high-sensitivity gamma spectrometry, the latter two methods so far never applied to archaeological artefacts of meteoritic origin.

2. Samples

The analyzed arrowhead is part of the collections of the Bern History Museum (No A/7396). It was found at Mörigen in the 19th century. Details of the recovery are not documented, but it is part of a series of arrowheads otherwise made of bronze, recovered in the mid-19th century, most likely during the excavations 1873/1874 led by Eduard v. Jenner and Edmund von Fellenberg. The sample was pictured as part of a series of bronze arrowheads from Mörigen by Bernatzky-Götze (1987), noting that it consists of iron, but without further investigation. The sample is shown in Fig. 1a and b. It has a mass of 2.904 g and dimensions of 39.3 mm (length), 25 mm (width) and 2.6 mm (maximum thickness). It consists of a tang (13 mm length) and a triangular blade. For comparative analyses, samples of the Twannberg meteorite from the Natural History Museum Bern (NMBE) were used, i.e. samples from Twannberg masses TW1 (NMBE 36467) and TW934 (NMBE 43747). Iron meteorite samples for establishing XRF calibrations for gallium and germanium were selected from the NMBE collection.

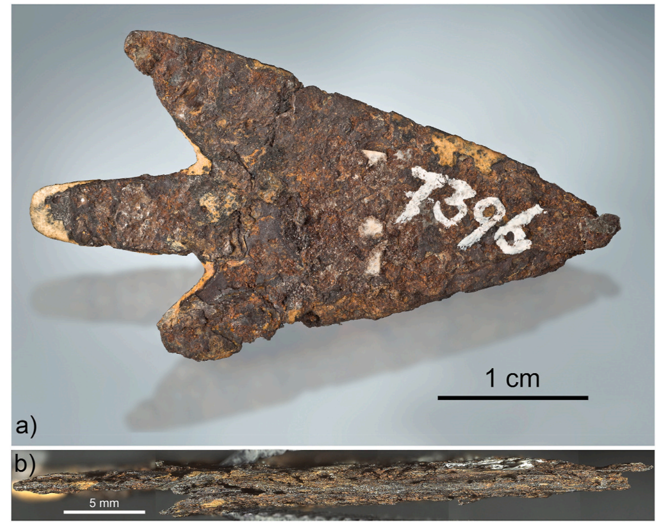

Fig. 1. a–b. a) Overview of the Mörigen arrowhead. Note adhering bright sediment material. Remnants of an older label on the left of the sample number. Total length is 39.3 mm. Photograph: Thomas Schüpbach. b) side view of the Mörigen arrowhead. Layered texture is well visible. Point is to the right.

3. Methods

3.1. Imaging and microscopy

Macroscopic images were obtained using a Nikon D800E camera followed by treating of image stacks with Helicon Focus software. Microscopic investigation of the Mörigen arrowhead was performed with a Leica MZ6 stereo microscope, a Keyence VHX-J20 digital microscope, a Leica DM4500P microscope in reflected light using crossed nicols, and a Leica M205C stereomicroscope with camera and Leica application suite image stacking software.

3.2. X-ray tomography

X-ray micro-computer tomography (micro-CT) was performed using a SkyScan 1273 instrument at the Institute of Geological Sciences of the University of Bern. The voltage of the X-ray source was set to 120 keV and the current to 125 μA. A filter of Cu (0.5 mm) was inserted between the source and the sample to reduce beam hardening. Alignment and flat field corrections were applied before acquisition. Raw images (attenuation) were obtained by rotating the object over 360° with a step of 0.3°. Raw images were made by averaging 5 successive acquisitions, each of them using an exposure time of 295 ms. The total scan duration was 1 h. Reconstruction of 1564 slice images was performed using the program NRecon version 1.7.5.1. Corrections for misalignment, ring artefacts and beam hardening were applied. The final voxel size on the reconstructed image is 25 μm, allowing the interpretation of any feature larger than ~100 μm. Further image analysis was performed using the software Dragonfly software, version 2021.1 for Windows (Object Research Systems (ORS) Inc, Montreal, Canada, 2021; software available at http://www.theobjects.com/dragonfly).

3.3. X-ray fluorescence

Screening of archaeological artefacts in collections was performed using a NITON GOLDD + portable X-ray analyzer equipped with a miniaturized X-ray tube with a silver anode, allowing the rapid (10 s counting time) identification of iron objects containing high (>1 wt%) concentrations of nickel typical of iron meteorites. The same instrument was used in the laboratory using long counting times, allowing the quantification of Ge and Ga. Concentrations of all elements except Ge and Ga are based on automated analysis by the Niton software, using in-house calibrations in the "Mining mode". The instrument was operated in the "Main Range", i.e. with Al/Fe filter at 50kV/40 μA. For the quantification of Ga and Ge, independent calibrations were established from spectral raw data using well-characterized iron meteorites as standards. Details of the calibration of Ga and Ge are given in Supplementary materials S3.1. No matrix correction was applied to analyses of Ga and Ge, as standards and unknowns had very similar bulk compositions. All analyses were performed with an analysis spot diameter of 8 mm and with a counting time of 120 s, and all elements including Ga and Ge were determined simultaneously on the same spots.

3.4. Muon induced X-ray emission (MIXE)

The depth-sensitive and non-destructive technique of Muon Induced X-ray Emission (MIXE) using the GermanIum Array for Non-destructive Testing (GIANT) setup was performed in the πE1 beamline at the Paul Scherrer Institute (PSI). A negative muon (μ^-) beam at a given muon momentum (p) was bombarded on the meteorite/arrowhead sample leading to the formation of muonic atoms at a particular depth inside the sample. Subsequently due to the de-excitation of the μ^- through the different muonic orbits, a cascade of muonic X-rays (μ-X rays) are emitted. When the μ^- is very near to the nucleus at the end of the de-excitation process, it might be captured by the nucleus leading to the production of gamma-rays (γ-rays). By changing the p, the penetration depth of the μ^- beam inside the sample can be controlled. In the πE1 beamline, the p can be varied from ~20 to 50 MeV/c leading to maximum penetration depths of a few centimeters (depending on the density of the sample under question). A detection limit of ~0.5 wt% has been achieved with the GIANT setup so far. In the case of the meteorite/arrowhead, the measurement time ranged from 5 h for p = 25 MeV/c to 1 h for p = 45 MeV/c. The MIXE technique has been previously applied at PSI to determine the elemental composition of a bronze archaeological sample (Biswas et al., 2023). The application of MIXE to meteorite samples (carbonaceous chondrites) have been performed in the accelerator facilities in Japan (Terada et al., 2014, 2017). Further details of this technique can be found in the Supplementary information S3.2. The interested readers can gather further information on the MIXE technique from Biswas et al. (2022), Gerchow et al. (2023) and the references therein.

3.5. Scanning electron microscopy (SEM)

Backscattered electron (BSE) and secondary electron (SE) images were recorded using a ZEISS EVO 50 scanning electron microscope at the Institute of Geological Sciences (University of Bern). Semi-quantitative elemental analyses were carried out by energy dispersive X-ray spectroscopy (EDX). The spectra have been measured with an acceleration voltage of 20 kV, a current of 950 pA and a working distance of 8.5 mm. The software EDAX TEAM has been used for standardless quantification using ZAF correction.

3.6. Gamma spectrometry

The content of radioisotopes in the sample was measured with gamma-spectrometry using the low-background GeMSE facility (Ramírez García et al., 2022; von Sivers et al., 2016). It is located at the Vue-des-Alpes tunnel, near Neuchâtel in Switzerland, under a rock overburden of 620 m water equivalent, which reduces the muon flux by a factor 2000 (Gonin et al., 2003). The instrument is used to identify materials and components to construct rare event search experiments for astroparticle physics (Aprile et al., 2022) and to determine the terrestrial age of meteorites (Rosén et al., 2019, 2021). GeMSE uses a coaxial p-type high-purity germanium crystal with a mass of 2.0 kg. The crystal is installed in an ultra-low background copper cryostat, which is kept at cryogenic temperatures with liquid nitrogen. The large sample cavity is shielded from ambient radioactivity by layers of oxygen-free copper as well as low-activity and standard lead. Radon in the sample cavity is removed by purging with boil-off nitrogen. Two large plastic scintillator panels are used to identify and reject muons. Nevertheless GeMSE's background is now muon-dominated (Ramírez García et al., 2022). Its low background level of (164 ± 2) counts/day in the 100–2700 keV interval allows the detection of radioisotopes at levels of a few tens of μBq/kg. We report activities in dpm/kg (decays per minute and kilogram; 1 dpm corresponds to 16.7 μBq) for better comparability with the meteorite literature.

3.7. Raman spectroscopy

Raman spectra were taken using a Jobin-Yvon LabRam HR-800 confocal instrument at the Institute of Geological Sciences, University of Bern. A Green (532.12 nm) Nd-YAG laser was used for signal excitation, focussed through an Olympus BX41 microscope with an Olympus 100/0.95 UM PlanFI objective lens.

4. Results

4.1. Search for meteoritic iron in archaeological collections

The search for iron objects with high nickel content in archaeological collections with objects from the area of Lake of Biel was done in two phases, a first one in 2013–2014 and a second one in 2021. During the first survey, iron objects of Bronze Age to La Tène Age were analyzed, the second approach was focused on iron objects of the late Bronze Age. A summary of the analyzed collections/materials is available as Supplementary materials Table S2. The large collections of the Laténium museum in Neuchâtel were previously searched for meteoritic artefacts by Jambon (2017) and inquiries showed that no additional iron objects of Bronze Age are identified in their collections. The arrowhead A/7396 from Mörigen (further: "Mörigen arrowhead", Fig. 1a and b), in the collection of the Bern History Museum is the only analyzed object with a significantly elevated nickel concentration (1.8–5.5 wt% Ni), as measured in the collection, compared with <1 wt% Ni for all other objects. The Mörigen arrowhead was analyzed and recognized as of meteoritic origin in the Bern History Museum on February 15, 2021.

4.2. Macroscopic and microscopic examination

The Mörigen arrowhead consists of rust-covered iron metal with a very pronounced laminated texture (Figs. 1b and 2). In some areas (Fig. 1a), fine-grained sediment is attached. Un-oxidized metal is visible only on a minor part of the otherwise rust-covered surface. The surface shows grinding/scratch marks in many places. In a few key areas the grinding marks clearly are present in a stratigraphic position below organic material and attached sediment. Remnants of a removed paper label and the sample number "7396" written in white letters are present on the surface (Fig. 1a).

4.3. X-ray tomography

The investigation by X-ray tomography showed that iron metal appears to form large parts of the surface areas while the oxidized (rust) layer is mostly very thin (<0.1 mm) and not well visible. A series of tomographic sections is shown in Fig. 2a and b. The crack observed by visual inspection is also clearly visible in the tomography, where it is shown to extend almost entirely across the blade of the arrowhead. The crack is filled with fine-grained silty sediment and iron (hydr)oxides, with some sand/silt grains clearly identifiable in the tomographs. One side of the arrowhead is clearly more massive with a thickness of the unoxidized metal of up to 1.2 mm, while the other side shows a maximum thickness of unoxidized metal of 0.6 mm (Fig. 2b). In addition to the main crack, more parallel fissures filled with oxidation products

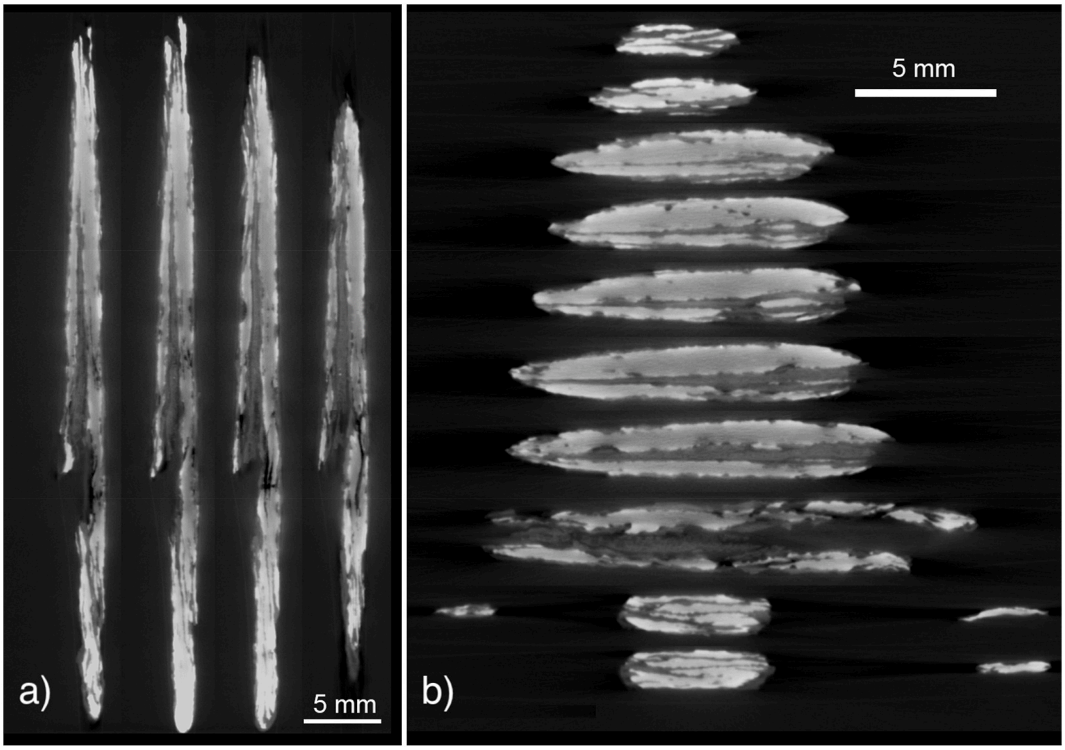

Fig. 2. a–b: X-ray tomographic sections of the Mörigen arrowhead. a) shows four sagittal sections, b) shows 10 transversal sections. Brightest (=densest) areas correspond to metallic iron, brightness of iron metal is variable due to flatness of the object. The layered structure and fractures filled with iron (hydr)oxides/sediment material resulting from oxidative volume expansion are well visible.

are clearly visible, in particular in the tang of the arrowhead (Fig. 2b). Overall, the material has a texture with a pronounced layering parallel to the frontal plane of the arrowhead. Such a preferred parallel layering is unusual in iron meteorites. It can be speculated that this might be a result of mechanical working of the specimen, representing a deformed Widmanstätten pattern.

4.4. *Bulk composition determined by X-ray fluorescence (XRF)*

The bulk composition of the Mörigen arrowhead was determined based on 18 measurements of 120 s duration each, covering both sides of the object, two analyses were exluded because they were influenced by sediment material. Supplementary materials Table S4 shows the concentration data for the 18 individual spots for all analyzed elements, and the elements relevant for meteorite characterization are summarized in Table 1 together with data for samples of the meteorites Kaalijarv, Morasko and Twannberg. The complete set of XRF results is contained in the supporting informations Table S4. It must be noted that the arrowhead with partial surface oxidation is a non-ideal object for XRF analysis. The observed variation in nickel concentrations (standard deviation of 22%) is much larger than of measurements on un-oxidized metal surfaces, most likely due to oxidation and possibly partial element mobility on the surface of the object. In addition to the typical meteoritic elements Fe, Ni, Co, Ga and Ge (Cr < 52 ppm, average detection limit), relatively high concentrations of As and Cu, not typical of iron meteorites, were determined. High concentrations of lead were measured only in the area of the white numbering, indicating the use of Pb-rich pigment for sample labeling. Analytical results for the other three European iron meteorites show that concentrations of Ni, Co, Ga and Ge are close to literature values (average relative deviations for Ni −1.2%, Co

Table 1
Compositional data for the Mörigen arrowhead, Kaalijärv, Morasko and Twannberg.

	Ni	Ni	Ni	Co	Co	Co	Ga	Ga	Ge	Ge	As	Cu
	wt.%	wt.%	wt.%	wt.%	wt.%	wt.%	ppm	ppm	ppm	ppm	ppm	ppm
	XRF	MIXE	Lit	XRF	MIXE	Lit	XRF	Lit	XRF	Lit	XRF	XRF
Mörigen arrowhead A/7396	7.12 ± 1.56	8.28 ± 0.22	–	0.85 ± 0.08	0.58 ± 0.02	–	135 ± 42	–	263 ± 78	–	585 ± 256	1039 ± 204
Kaalijärv	8.03 ± 0.13	–	7.55	0.88 ± 0.05	–	0.48	96 ± 18	80	318 ± 14	293	–	–
Morasko	6.38 ± 0.15	–	6.76	0.43 ± 0.04	–	0.45	89 ± 17	103	499 ± 22	500	–	–
Twannberg TW1	4.19 ± 0.22	4.64 ± 0.16[a]	4.52	0.63 ± 0.16	0.59 ± 0.02[a]	0.52	49 ± 9	35	51 ± 2	49	–	–
Twannberg TW934, 1 mm depth	–	4.51 ± 0.42	4.52	–	0.55 ± 0.07	0.52	–	–	–	–	–	–

Lit: Reference values from the literature (Wasson and Kallemeyn 2002 for Kaalijärv and Morasko; Hofmann et al., 2009 for Twannberg).
[a] Average of 0–1 mm depth.

+33%, Ga +5%, Ge +9%). Cobalt values as determined by XRF have relatively large errors due to overlaps of the Fe K_{β} and Co K_{α} lines.

4.5. Muon induced X-ray emission spectrometry (MIXE)

For comparison with the arrowhead and to test the effect of surficial oxidation layers on meteoritic iron, analyses were also performed on unoxidized (TW1, fresh cut) and oxidized (TW 934) samples of the Twannberg meteorite (Table 2). First, the analyses of the unoxidized Twannberg meteorite show a very good agreement with published data (Hofmann et al., 2009). Second, the analyses of surficially oxidized Twannberg sample TW 934 show a systematic increase in Ni concentration with increasing muon momentum/energy (and hence depth), reaching a concentration of 4.51 wt% for highest energies, again very similar to published values for pure metal. The location of analysis was selected based on X-ray tomographic sections at a place with a rust layer thickness of 0.5–1.5 mm. Sample TW 934 is uncut and completely covered by a rust layer with preserved fusion crust at some places.

Analysis of the arrowhead by MIXE was performed on May 5–6, 2022. A beam diameter of ~2 cm was used, and the side with labelling/paint was analyzed because this side shows a larger metal thickness above the pervasive crack visible in the tomography. Fig. 3 shows the μ-X ray spectra of the arrowhead (blue) compared with the oxidized (red) and unoxidized (green) Twannberg samples. All the μ X-rays of Fe, Ni, and Co along with the γ-rays are marked in this figure. The elevated Ni content of the arrowhead relative to Twannberg is evident. Concentrations of Ni and Co, in the arrowhead, obtained by MIXE are 8.22–8.36 wt% Ni and 0.56–0.61 wt% Co. A comparison of the Ni and Co concentrations in all the three measured samples is shown in Fig. 4. The

Table 2
MIXE analytical data for Twannberg meteorites and Mörigen arrowhead.

(Based on relative areas of Kα peaks normalized to e-e + annihilation peak)						
Unoxidized Twannberg meteorite (TW1)						
Muon momentum (MeV/c)	25	30	35	40	45	average
Depth (mm)	0.1 ± 0.03	0.23 ± 0.11	0.42 ± 0.10	0.70 ± 0.16	1.1 ± 0.2	0.1–1.1 mm
Fe wt.%	94.62 ± 4.76	94.72 ± 5.38	94.84 ± 3.64	94.78 ± 4.10	94.88 ± 4.21	94.77 ± 1.99
Ni wt.%	4.73 ± 0.27	4.69 ± 0.30	4.59 ± 0.31	4.64 ± 0.43	4.55 ± 0.39	4.64 ± 0.16
Co wt.%	0.65 ± 0.05	0.59 ± 0.05	0.57 ± 0.03	0.58 ± 0.05	0.57 ± 0.05	0.59 ± 0.02
Twannberg meteorite with oxide layer (TW934)						
Muon momentum (MeV/c)	25	30	35	40	45	average
Depth (mm)	0.1 ± 0.03	0.23 ± 0.11	0.42 ± 0.10	0.70 ± 0.16	1.1 ± 0.2	0.1–1.1 mm
Fe wt.%	96.00 ± 4.89	95.66 ± 11.59	95.88 ± 2.67	95.20 ± 11.15	94.94 ± 4.53	95.53 ± 3.52
Ni wt.%	3.42 ± 0.26	3.79 ± 0.42	3.55 ± 0.12	4.19 ± 0.52	4.51 ± 0.42	3.89 ± 0.17
Co wt.%	0.58 ± 0.06	0.56 ± 0.07	0.58 ± 0.03	0.61 ± 0.08	0.55 ± 0.07	0.57 ± 0.03
Mörigen arrowhead A/7396						
Muon momentum (MeV/c)	25	30	35	40	45	average
Depth (mm)	0.1 ± 0.03	0.23 ± 0.11	0.42 ± 0.10	0.70 ± 0.16	1.1 ± 0.2	0.1–1.1 mm
Fe wt.%	91.04 ± 8.64	91.15 ± 2.86	91.11 ± 2.70	91.15 ± 4.12	91.23 ± 5.26	91.14 ± 2.32
Ni wt.%	8.36 ± 0.72	8.27 ± 0.38	8.31 ± 0.28	8.24 ± 0.38	8.22 ± 0.55	8.28 ± 0.22
Co wt.%	0.60 ± 0.06	0.58 ± 0.02	0.58 ± 0.02	0.61 ± 0.07	0.56 ± 0.07	0.58 ± 0.02

MIXE analyses confirm concentrations of Ni and Co characteristic of iron meteorites (e.g. Buchwald 1975; Scott 2020). Concentrations of Ni, typically depleted in oxidation products relative to fresh metal, do not systematically vary with muon energy (depth), indicating that the oxidation layer is very thin, which is consistent with the tomography results and the observation of metallic iron in some areas on the surface. The MIXE analyses yielding similar nickel concentrations independent of muon energy (depth) also demonstrate that the high nickel concentrations determined by XRF are not due to a secondary surficial enrichment related to weathering.

1100–1800 keV for the arrowhead (blue), the oxidized Twannberg iron meteorite (red), and the unoxidized Twannberg iron meteorite (green). The muonic X-rays (μ-X rays) of Fe, Ni and Co are marked. The higher concentration of nickel in the arrowhead is clearly showing up in the Ni K_{α} and $K_{\beta 1}$ peaks.The gamma rays (γ-rays), resulting from the nuclear capture of muons in Fe and Ni nuclei are also shown.

4.6. SEM analyses

Specific areas exposed on the Mörigen arrowhead were imaged with the SEM using backscattered and secondary electron imaging, and standardless elemental analyses were carried out on exposed metal, organic material, adhering sediment and labelling. Point analyses of randomly selected areas of exposed metal clearly show the presence of both the nickel-rich iron phase taenite (Fe 66.3 ± 4.0, Ni 33.3 ± 4.1, Co 0.38 ± 0.23 wt%, n = 13) and of nickel-poor kamacite (Fe 92.7 ± 1.0, Ni 6.66 ± 1.04, Co 0.68 ± 0.28 wt%, n = 39). Morphologically taenite is only distinguishable from kamacite in a few cases, e.g. as thin band in otherwise oxidized iron (Fig. 5A). Organic material was detected by its dark appearance in backscatter imaging mode (Fig. 5B,C). Point analyses show a high content of carbon with low concentrations of oxygen. Analyses of the adhering sediment showed this to be rich in Ca, C and O with admixed Si, consistent with calcium carbonate and quartz grains. In the backscatter imaging mode, the inventory number (7396) clearly proved to be composed of material with a high atomic number (Z), overwritten with a later paint having a low average Z. Point analyses showed the former to be lead-rich, the latter rich in Ti with individual particles rich in Sb. Imaging in the secondary ion mode of areas close to the adhering sediment confirmed the presence of striations on the metal/oxide surface clearly leading under the sediment (Fig. 5C,D), as observed with optical microscopy.

4.7. Gamma spectrometry

Gamma spectrometry of the Mörigen arrowhead was performed at the GeMSE facility between November 2021 and January 2022. The measured gamma spectrum acquired over 63 live-days is shown in Fig. 6 together with the background spectrum without sample. The detection efficiency was determined with the Geant4 simulation toolkit (Agostinelli et al., 2003) utilizing the 3D scan of the sample obtained from the X-ray tomography. The statistical evaluation employs Bayesian statistics as detailed in von Sivers et al. (2016). The Bayes Factor (BF) is used to evaluate the statistical significance of a signal (assuming flat and equal priors). As in Rosén et al. (2019), we treat activities with BF <0.33 as detected signals (positive evidence according to Kass and Raftery, 1995). For ^{26}Al at 1808.7 keV we infer BF = 0.00015 and determine an activity of $1.7^{+0.5}_{-0.4}$ dpm/kg. We also detect ^{40}K, ^{238}U, and ^{228}Th with activities of 330^{+19}_{-15} dpm/kg, 150^{+18}_{-20} dpm/kg, and $18.1^{+1.0}_{-0.8}$ dpm/kg, respectively. Upper limits of 0.66 dpm/kg and 1.5 dpm/kg are placed on the activity of ^{60}Co and ^{137}Cs at 95%CL, respectively.

4.8. Raman spectroscopy

Raman spectra of black organic material located clearly in a situation below adhering sediment on the arrowhead show broad peaks centered

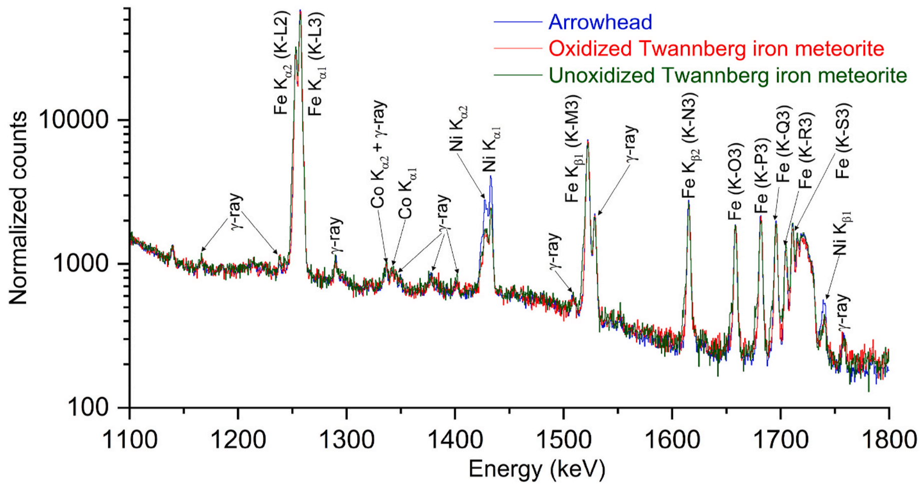

Fig. 3. Normalized spectra for muon momentum p = 30 MeV/c, in the energy range.

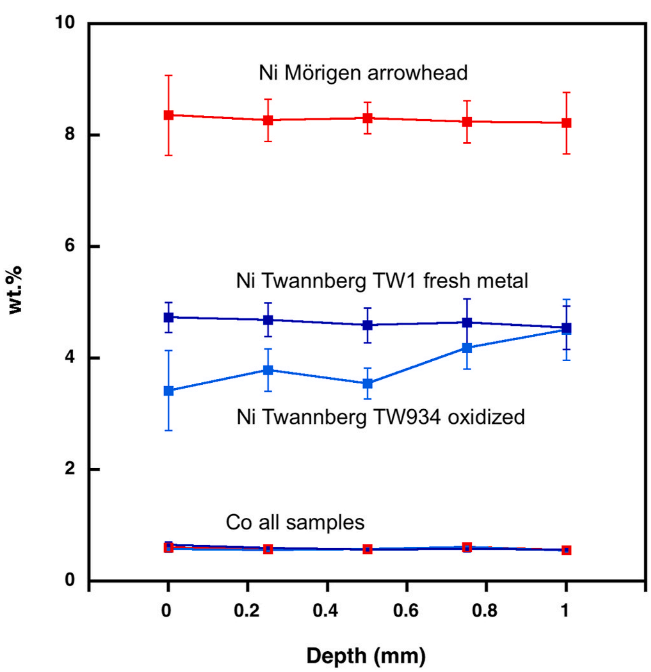

Fig. 4. Nickel and cobalt concentrations as a function of depth (muon momentum) for the Mörigen arrowhead (red), compared with unoxidized Twannberg TW1 meteorite (dark blue) and oxidized Twannberg TW 934 meteorite (light blue). Cobalt shows very similar values in all samples and depths. Individual data points are connected by lines to depict the trend in different samples.

at Raman shifts of ~1350 cm^{-1} and ~1600 cm^{-1}, characteristic for oxygen-poor tar-like materials (Trabska et al., 2011).

5. Discussions

5.1. Interpretation of the shape and surface morphology

The Mörigen arrowhead is a very flat object (aspect ratio 15.1, after correction for thickness increase due to oxidation ~20). Primary shapes of meteoritic iron are never as flat, even in case of “shrapnels” (fragments formed due to explosive disruption on impact). The flat aspect of the object must be due to artificial deformation of an originally less flattened object, either due to cold or hot working. This is consistent with the layered nature evident from the X-ray tomographs, most likely resulting from a deformed Widmanstätten pattern. Cold-working of meteoritic iron is well documented from Greenland, where it has been the only method over possibly 1000 years (~800–1800 AD) for preparing tools from the Cape York meteorite. The resulting tools show a characteristic highly layered microstructure (Buchwald 1992) resulting from flattening of rather large kamacite and taenite grains. Hot working cannot be excluded, because the Ni-rich taenites band will survive even though recrystallization is likely above ~700 °C (depending on Ni content), but recrystallization is not recognizable with the non-destructive techniques applied here. Based on the presence of both Ni-poor and Ni-rich iron metal, the layered structure most likely represents a deformed Widmanstätten pattern characteristic for octahedritic meteorites. The observed grinding marks present in a situation below attached organic material and sediment clearly demonstrate that these grinding marks are due to the shape-giving process of the arrowhead and not due to a cleaning procedure after the find that probably caused surficial grinding marks and exposure of unoxidized metal. The style of the iron arrowhead strongly resembles that of bronze arrowheads from the same find complex, even though the fabrication process was very different. The attached carbon-rich organic material likely represents remnants of tar, probably wood (birch?) tar, indicating that it was fastened to an arrow at some point.

5.2. Bulk composition, meteoritic nature and type of meteorite

The concentrations of Ni, Co, Ga and Ge (Table 1), mass ratios of Ni/Fe (0.08–0.09) and Ni/Co (8.3–14.3 as compared with Figs. 1 and 3 in Jambon (2017), the presence of kamacite and taenite, and the detection of cosmogenic ^{26}Al unambiguously demonstrate the meteoritic nature of the Mörigen arrowhead. The coexistence of the two iron phases shows that the meteorite is an octahedrite, in contrast to the nearby Twannberg meteorite that only contains kamacite. Nickel and germanium concentrations are most compatible with the IAB iron meteorite complex (Fig. 7), a relatively common group of iron meteorites (367 approved meteorites, Meteoritical Society database accessed May 22, 2023), often representing large falls such as Cañon Diablo (Arizona) or Campo de Cielo (Argentina). MIXE analyses of the arrowhead and of Twannberg sample TW934 demonstrate that the nickel concentration of the metal below the oxidation layer is very different in the two samples, corresponding to 8.2 wt% in the arrowhead and 4.5 wt% in TW934. Within analytical error, elemental concentrations might also correspond to an iron meteorite of group IC, but this is a very rare group with only 13 approved meteorites and no IC meteorite is known from Europe. Ni concentrations in IC meteorites are 6.55 ± 0.25 wt %. There is no compositional overlap with other groups of iron meteorites.

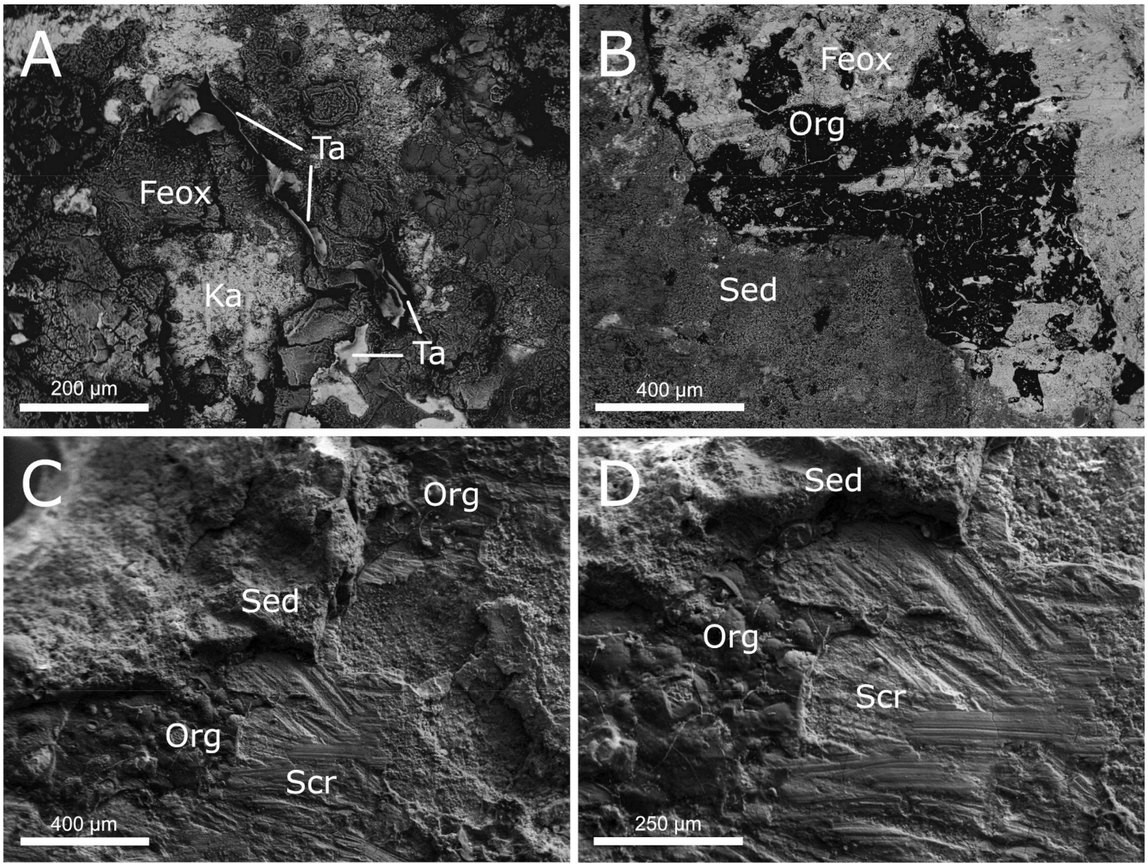

Fig. 5. SEM images of typical surface areas of the arrowhead. A) Thin lamina of taenite (Ta) surrounded by oxidation products (Feox) and nearby kamacite (Ka), BSE image; B) Fe oxidation products (Feox) covered by organic material, probably birch tar (Org, dark) and a latest layer of adhering sediment (Sed), BSE image. C, D) Scratched surface (Scr) below organic material (wood tar; Org) and sediment (Sed). SE images.

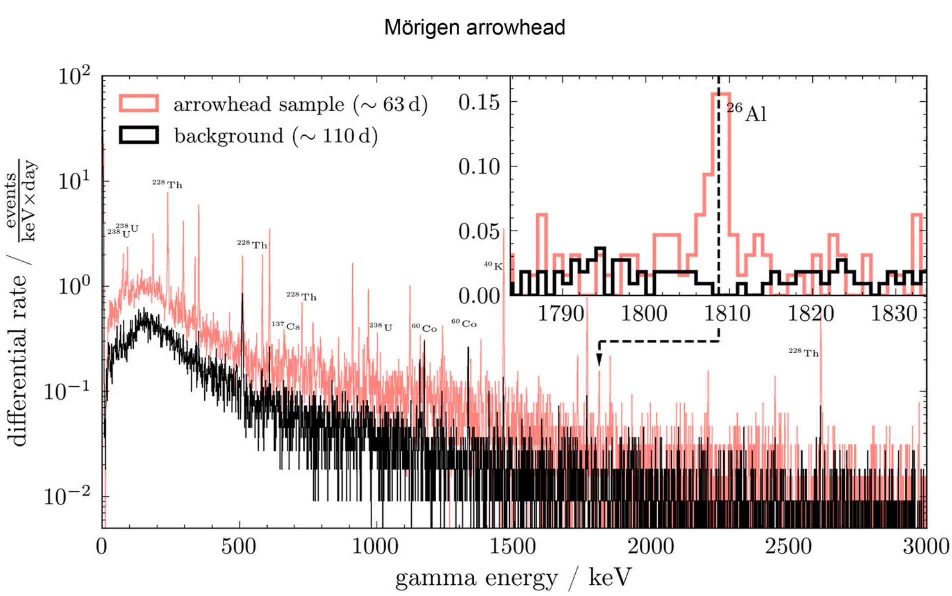

Fig. 6. Gamma-ray spectrum of the Mörigen arrowhead obtained at the GeMSE underground laboratory. The inset shows the small but significant peak of cosmogenic ^{26}Al at 1808.7 keV.

5.3. Gamma spectrometry data and pre-atmospheric mass of the parent meteorite

The presence of cosmogenic ^{26}Al unambiguously proves the meteoritic origin of the Mörigen arrowhead. Based on model calculations (Leya and Masarik 2009), the activity of cosmogenic ^{26}Al in freshly fallen iron meteorites with diameters up to 60 cm is in the range of 2.3–4.8 dpm/kg, consistent with activities measured in meteorites, e.g. by Smith et al. (2019). In the latter study activities of up to 4.7 dpm/kg (mean 2.5 ± 1.1 dpm/kg, median 2.8 dpm/kg; n = 52) were determined

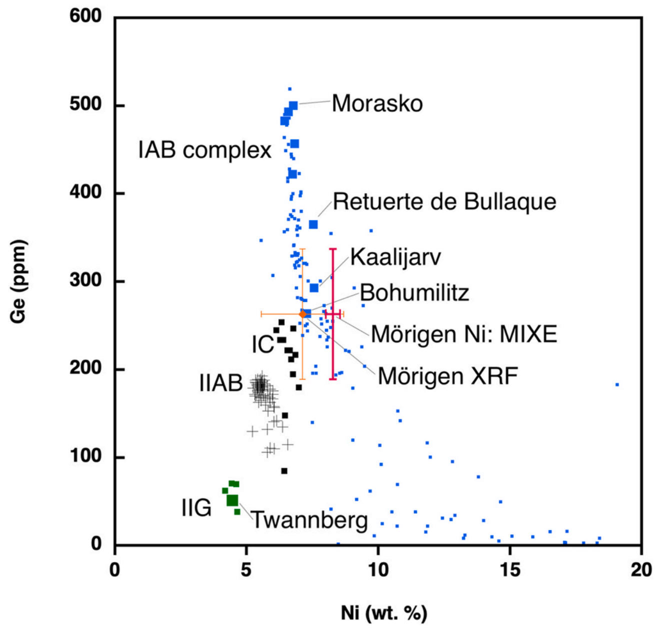

Fig. 7. XRF and MIXE bulk Ni and Ge concentrations for the Mörigen arrowhead (data from Tables 1 and 2), compared with compositional data for the IAB iron meteorite complex (blue filled squares), IC (black squares), IIAB (black crosses) and IIG (green filled squares) meteorites. Meteorite data from Wasson and Kallemeyn (2002), Scott and Wasson (1976), Wasson et al. (2007), Wasson and Choe (2009), Hofmann et al. (2009). Large IAB iron meteorites from Europe are plotted with larger blue squares.

in iron meteorites. The comparatively low activity of cosmogenic ^{26}Al of $1.7^{+0.5}_{-0.4}$ dpm/kg in the Mörigen arrowhead demonstrates that the parent meteorite was more strongly shielded from galactic cosmic rays in space than an average iron meteorite, i.e. the sample must have been surrounded by a significant mass of meteoritic material. The measured activity constrains the pre-atmospheric diameter of the meteorite (conservatively assuming a spherical shape) to a minimum of ~80 cm corresponding to a minimum mass of ~2 tons (based on Leya and Masarik 2009) because smaller meteorites show higher activities even in the center. The activities of ^{40}K and U/Th-series nuclides are interpreted as the result of contamination with terrestrial mineral matter, visible in the microscopic and tomographic images (Figs. 1 and 2).

5.4. Alteration and non-meteoritic materials

The most obvious alteration of the arrowhead is oxidation of the iron. The elements As and Cu, determined in concentrations of 590 and 1000 ppm, respectively, are present in iron meteorites in concentrations of less than 100 ppm and might be derived from remnants of ore/bronze working in the host sediment, or perhaps more likely, to contamination by dust during storage together with objects rich in these elements. The fact that metallic iron, including more easily oxidizing kamacite is exposed on the surface, and the presence of surficial scratch marks (in addition to clearly older ones) show that the arrowhead was quite strongly cleaned after the find, probably in order to remove some of the rust.

The organic material stratigraphically located clearly between meteoritic iron/rust and overlying sediment material shows the characteristics of wood tar based on colour, lustre (optical microscopy), main chemical constituents (SEM-EDX) and Raman peak positions (Trabska et al., 2011).

High concentrations of lead were measured with pXRF in the area of the white inventory number. Follow-up EDX-analyses showed that the sample number was first written with a lead-rich pigment, later corrected or repaired with an ink rich in titanium white containing an admixture of antimony (probably as oxide).

5.5. Possible linking of the Mörigen arrowhead with known meteorites

The Mörigen arrowhead must be derived from a large (minimum 2 tons pre-atmospheric mass) IAB iron meteorite based on gamma spectrometry and elemental composition. Among large IAB meteorites from Europe, three have a chemical composition consistent with the Mörigen arrowhead (Fig. 7): Bohumilitz (Czech Republic), Retuerte de Bullaque (Spain) and Kaalijarv (Estonia). Kaalijarv is a large meteorite that produced a series of impact craters (the largest, called Kaalijärv, is 110 m in diameter, note different spelling for meteorite and crater) on the island of Saarema in Estonia (Rasmussen et al., 2000; Veski et al., 2001, 2004; Losiak et al., 2016). As a result of the explosive impact, most of the meteorite mass (probably several 100 tons) was destroyed and recovered meteorite fragments are mostly small "shrapnels" (Buchwald 1975) resulting from the destruction of the main mass. Such a small fragment may be the source of the arrowhead, but detachment from larger masses is also possible, as is well documented for the Cape York meteorite (Buchwald 1975, 1992, 2005). The total recovered mass of Kaalijarv is in the order of ~10 kg only (Buchwald 1975, Wesel, 2004–2019). Based on three independent studies of organic materials from the base of lake sediments and below ejecta, the impact most likely occurred between 1870 and 1440 BCE, i.e. during the Bronze Age (Saarse et al., 1991; Veski et al., 2004; Losiak et al., 2016). Other impact ages of ~6400 BCE (Raukas 2000) and 800-400 BCE (Rasmussen et al., 2000) are from impact features observed in peat bogs at several km distance and appear less reliable due to the uncertain correlation and inconsistency. Among the known large and compositionally fitting IAB meteorites in Europe, Kaalijarv is the most likely candidate because of its Bronze Age impact age. Even though larger than the minimum pre-atmospheric diameter estimated from ^{26}Al in the Mörigen arrowhead, a pre-atmospheric radius of an estimated few meters still allows the presence of significant proportions of the meteorite having ^{26}Al activities in the analyzed range. Kaalijarv likely was the most obvious appearance of a meteorite during the Bronze Age in Europe because the impact occurred in an inhabited area (Veski et al., 2001, 2004; Plado 2012; Losiak et al., 2016). We thus consider that Kaalijarv is a possible source for the meteoritic iron from which the Mörigen arrowhead was produced, but other meteorites cannot be excluded. The known masses of other large IAB meteorites from Europe with fitting chemistry (Bohumilitz, Retuerta de Bullaque) are only marginally large enough to be consistent with the estimated shielding, but they could be part of larger, yet undiscovered strewn fields. The Morasko IAB strewn field in Poland, also with craters of up to 90 m diameter and with a young impact age (~3000 BC, EStankowski, 2001; Szokaluk et al., 2019), can be excluded as a source because of the very high content of germanium of ~500 ppm (Wasson et al., 2007, Table 1, Fig. 7). Among other meteoritic iron artefacts from Europe, the objects from Wietrzno (axe) and Czestochowa-Rakowa (bracelets) are closest in location and time, but unrelated, because they were made from a clearly different, more Ni-rich meteorite (Kotowiecki 2004; Jambon 2017).

6. Conclusions

The fact that a search for meteoritic iron among archaeological artefacts in near proximity of the large Twannberg strewn field only yielded a single object made from a clearly different meteorite, indicates that Twannberg meteorites may not have been known during the Bronze Age and buried meteorites were not easily identified at that time. The identified arrowhead made from IAB meteoritic iron from a Bronze Age settlement at Mörigen, Switzerland, demonstrates that iron meteorites were used and traded by 800 BCE (or earlier) in Central Europe. Based on Ni–Ge concentrations and shielding derived from ^{26}Al activity of the arrowhead, the Kaalijarv (Estonia) meteorite with a Bronze Age impact age (~1500 BCE) appears to be a possible source candidate, implying a transport over ~1600 km. Fragments of this meteorite may have been traded over the same routes from the Baltic area as amber (Kaul and Vrarberg 2017). Whether or not derived from Kaalijarv, the arrowhead most likely was not a singular object and likely other worked fragments of meteoritic iron, including samples of relatively small size, are present in archaeological collections in Europe and possibly even at larger distance. A small size of such objects appears to be a likely possibility because of the many "shrapnels" that resulted from the impact of the Kaalijarv meteorite, but larger specimens may have been used as well. Other Bronze Age artefacts made from meteorites, in particular small ones with a very flat aspect such as the "chisels" in the grave of Tutankhamun (Ströbele et al., 2016; Broschat et al., 2018, 2022) should be subjected to comparative analyses. The fact that searches in archaeological collections in Estonia have not been successful (Tamm 2014, Jüri Plado, pers. comm. 2021) may be due to the mainly small size of iron fragments resulting from the impact. The search for related iron fragments of meteoritic origin in collection should thus include (but not be limited to) small and flat objects.

This study demonstrates that the application of purely non-destructive methods can yield a wide range of information about archaeological artefacts made of (suspected) meteoritic iron. Muon Induced X-ray Emission (MIXE) is a particularly useful technique to determine the primary nickel content of iron below a thin rust layer, and gamma spectrometry can provide definitive proof of meteoritic origin and information about the size of the meteorite from which artefacts are derived. X-ray fluorescence is demonstrated to be useful for quantification of the characteristic meteoritic elements Ga and Ge in iron metal at levels above tens of ppm.

Declaration of competing interest

The authors declare the following financial interests/personal relationships which may be considered as potential competing interests: Alex Amato reports financial support was provided by Swiss National Science Foundation.

Acknowledgements

All the institutions that provided access to their collections during the search for meteoritic artefacts are gratefully acknowledged: Historisches Museum Bern, Archäologischer Dienst des Kantons Bern, Schweizerisches Nationalmuseum, Neues Museum Biel, Schlossmuseum Burgdorf, Museum Irlet Twann, Pfahlbaumuseum Lüscherz, Musée d'art et d'histoire Genève. Jüri Plado from the University of Tartu provided valuable information and a sample of the Kaalijarv meteorite. Lukas Smula is thanked for samples of the Morasko meteorite. MIXE analyses were performed as part of the Swiss National Science Foundation Synergia project "Deepμ", Grant: 193691. The use of germanium detectors from Technical University Munich, Joint Institute for Nuclear Research Dubna and Osaka University is gratefully acknowledged. We also acknowledge the muX collaboration for using their equipments and data acquisition codes. We thank our colleagues at the Laboratory for High Energy Physics/Albert Einstein Center, University of Bern, for their continuous support to operate the GeMSE facility. The gamma-spectrometry analysis was supported by the European Research Council (ERC) grant No. 724320 (ULTIMATE). The micro-CT analysis was supported by the European Research Council (ERC) under the European Union's Horizon 2020 research and innovation program (Grant agreement No. 850530). We thank Chr. Koeberl and two anonymous reviewers for their very constructive comments.

Appendix A. Supplementary data

Supplementary data to this article can be found online at https://doi.org/10.1016/j.jas.2023.105827.

References

Agostinelli, S., Allison, J., Amako, K., Apostolakis, J., Araujo, H., Arce, P., Asai, M., Axen, D., Banerjee, S., Barrand, G., Behner, F., Bellagamba, L., Boudreau, J., Broglia, L., Brunengo, A., Burkhardt, H., Chauvie, S., Chuma, J., Chytracek, R., Cooperman, G., Cosmo, G., Degtyarenko, P., Dell'Acqua, A., Depaola, G., Dietrich, D., Enami, R., Feliciello, A., Ferguson, C., Fesefeldt, H., Folger, G., Foppiano, F., Forti, A., Garelli, S., Giani, S., Giannitrapani, R., Gibin, D., Gómez Cadenas, J., González, I., Gracia Abril, G., Greeniaus, G., Greiner, W., Grichine, V., Grossheim, A., Guatelli, S., Gumplinger, P., Hamatsu, R., Hashimoto, K., Hasui, H., Heikkinen, A., Howard, A., Ivanchenko, V., Johnson, A., Jones, F., Kallenbach, J., Kanaya, N., Kawabata, M., Kawabata, Y., Kawaguti, M., Kelner, S., Kent, P., Kimura, A., Kodama, T., Kokoulin, R., Kossov, M., Kurashige, H., Lamanna, E., LampÅLen, T., Lara, V., Lefebure, V., Lei, F., Liendl, M., Lockman, W., Longo, F., Magni, S., Maire, M., Medernach, E., Minamimoto, K., Mora de Freitas, P., Morita, Y., Murakami, K., Nagamatu, M., Nartallo, R., Nieminen, P., Nishimura, T., Ohtsubo, K., Okamura, M., O'Neale, S., Oohata, Y., Paech, K., Perl, J., Pfeiffer, A., Pia, M., Ranjard, F., Rybin, A., Sadilov, S., Di Salvo, E., Santin, G., Sasaki, T., Savvas, N., Sawada, Y., Scherer, S., Sei, S., Sirotenko, V., Smith, D., Starkov, N., Stoecker, H., Sulkimo, J., Takahata, M., Tanaka, S., Tcherniaev, E., Safai Tehrani, E., Tropeano, M., Truscott, P., Uno, H., Urban, L., Urban, P., Verderi, M., Walkden, A., Wander, W., Weber, H., Wellisch, J., Wenaus, T., Williams, D., Wright, D., Yamada, T., Yoshida, H., Zschiesche, D., 2003. Geant4—a simulation toolkit. Nucl. Instrum. Methods Phys. Res. Sect. A Accel. Spectrom. Detect. Assoc. Equip. 506, 250–303. https://doi.org/10.1016/S0168-9002(03)01368-8.

Aprile, E., Abe, K., Agostini, F., Maouloud, S.A., Alfonsi, M., Althueser, L., Angelino, E., Angevaare, J.R., Antochi, V.C., Martin, D.A., Arneodo, F., Baudis, L., Baxter, A.L., Bellagamba, L., Biondi, R., Bismark, A., Brown, A., Bruenner, S., Bruno, G., Budnik, R., Capelli, C., Cardoso, J.M.R., Cichon, D., Cimmino, B., Clark, M., Colijn, A.P., Conrad, J., Cuenca-García, J.J., Cussonneau, J.P., D'Andrea, V., Decowski, M.P., Gangi, P.D., Pede, S.D., Giovanni, A.D., Stefano, R.D., Diglio, S., Elykov, A., Farrell, S., Ferella, A.D., Fischer, H., Fulgione, W., Gaemers, P., Gaior, R., Galloway, M., Gao, F., Glade-Beucke, R., Grandi, L., Grigat, J., Higuera, A., Hils, C., Hiraide, K., Hoetzsch, L., Howlett, J., Iacovacci, M., Itow, Y., Jakob, J., Joerg, F., Kato, N., Kavrigin, P., Kazama, S., Kobayashi, M., Koltman, G., Kopec, A., Landsman, H., Lang, R.F., Levinson, L., Li, I., Liang, S., Lindemann, S., Lindner, M., Liu, K., Lombardi, F., Long, J., Lopes, J.A.M., Ma, Y., Macolino, C., Mahlstedt, J., Mancuso, A., Manenti, L., Manfredini, A., Marignetti, F., Undagoitia, T.M., Martens, K., Masbou, J., Masson, D., Masson, E., Mastroianni, S., Messina, M., Miuchi, K., Mizukoshi, K., Molinario, A., Moriyama, S., Morå, K., Mosbacher, Y., Murra, M., Ni, K., Oberlack, U., Palacio, J., Peres, R., Pienaar, J., Pierre, M., Pizzella, V., Plante, G., Qi, J., Qin, J., GarcÅLıa, D.R., Reichard, S., Rocchetti, A., Rupp, N., Sanchez, L., dos Santos, J.M.F., Sartorelli, G., Schreiner, J., Schulte, D., Schulze Eißing, H.S., Schumann, M., Lavina, L.S., Selvi, M., Semeria, F., Shagin, P., Shockley, E., Silva, M., Simgen, H., Takeda, A., Tan, P.L., Terliuk, A., Therreau, C., Thers, D., Toschi, F., Trinchero, G., Tunnell, C., Tönnies, F., Valerius, K., Volta, G., Wei, Y., Weinheimer, C., Weiss, M., Wenz, D., Westermann, J., Wittweg, C., Wolf, T., Xu, Z., Yamashita, M., Yang, L., Ye, J., Yuan, L., Zavattini, G., Zhang, Y., Zhong, M., Zhu, T., Zopounidis, J.P., Laubenstein, M., Nisi, S., 2022. Material radiopurity control in the XENONnT experiment. The European Physical Journal C 82, 599. https://doi.org/10.1140/epjc/s10052-022-10345-6.

Bernatzky-Götze, M., 1987. Mörigen - die spätbronzezeitlichen Funde, vol. 16. Antiqua, Basel.

Biswas, S., Gerchow, L., Luetkens, H., Prokscha, T., Antognini, A., Berger, N., Cocolios, T. E., Dressler, R., Indelicato, P., Jungmann, K., Kirch, K., Knecht, A., Papa, A., Pohl, R., Pospelov, M., Rapisarda, E., Reiter, P., Ritjoho, N., Roccia, S., Severijns, N., Skawran, A., Vogiatzi, S.M., Wauters, F., Willmann, L., Amato, A., 2022. Characterization of a continuous muon source for the non-destructive and depth-selective elemental composition analysis by muon induced x- and gamma rays. Appl. Sci. 2022 12, 2541. https://www.mdpi.com/2076-3417/12/5/2541.

Biswas, S., Megatli-Niebel, I., Raselli, L., Simke, R., Cocolios, T.E., Deokar, N., Elender, M., Gerchow, L., Hess, H., Khasanov, R., Knecht, A., Luetkens, H., Ninomiya, K., Papa, A., Prokscha, T., Reiter, P., Sato, A., Severijns, N., Shiroka, T., Seidlitz, M., Vogiatzi, S.M., Wang, C., Wauters, F., Warr, N., Amato, A., 2023. The non-destructive investigation of a late antique knob bow fibula (Bügelknopffibel) from Kaiseraugst/CH using Muon Induced X-ray Emission (MIXE). Heritage Science 11, 43. https://doi.org/10.1186/s40494-023-00880-0.

Bjorkman, J.K., 1973. Meteors and meteorites in the ancient near east. Meteoritics 8, 91–130. https://onlinelibrary.wiley.com/doi/abs/10.1111/j.1945-5100.1973.tb00146.x.

Broschat, K., Ströbele, F., Koeberl, C., Eckmann, C., Mertah, E., 2018. Himmlisch! Die Eisenobjekte aus dem Grab des Tutanchamun. Forschungen am Römisch-Germanischen Zentralmuseum 15, 1–59.

Broschat, K., Ströbele, F., Koeberl, C., Eckmann, C., Mertah, E., Schutz, M., 2022. Iron from Tutankhamun's Tomb. The American University in Cairo Press, pp. 1–76.

Buchwald, V.F., 1975. Handbook of Iron Meteorites. University of California Press, Berkeley.

Buchwald, V.F., 1992. On the use of iron by the eskimos in Greenland. Mater. Char. 29, 139–176. http://www.sciencedirect.com/science/article/pii/104458039290112U.

Buchwald, V.F., 2005. Iron and Steel in Ancient Times. Royal Danish Academy of Sciences and Letters, Copenhagen.

Chen, K., Wang, Y., Liu, Y., Mei, J., Jiang, T., 2018. Meteoritic origin and manufacturing process of iron blades in two Bronze Age bimetallic objects from China. J. Cult. Herit. 30, 45–50.

Comelli, D., D'Orazio, M., Folco, L., El-Halwagy, M., Frizzi, T., Alberti, R., Capogrosso, V., Elnaggar, A., Hassan, H., Nevin, A., Porcelli, F., Rashed, M.G.,

Valentini, G., 2016. The meteoritic origin of Tutankhamun's iron dagger blade. Meteoritics Planet. Sci. 51, 1301–1309. https://onlinelibrary.wiley.com/doi/full/10.1111/maps.12664.
Gerchow, L., Biswas, S., Janka, G., Vigo, C., Knecht, A., Vogiatzi, S.M., Ritjoho, N., Prokscha, T., Luetkens, H., Amato, A., 2023. Germanium array for non-destructive testing (GIANT) setup for muon induced X-ray emission (MIXE) at the Paul Scherrer Institute. Rev. Sci. Instrum. 94, 045106. https://pubs.aip.org/aip/rsi/article/94/4/045106/2877786/GermanIum-array-for-non-destructive-testing-GIANT.
Gonin, Y., Busto, J., Vuilleumier, J.L., 2003. The "La Vue-des-Alpes" underground laboratory. Rev. Sci. Instrum. 74, 4663–4666. https://doi.org/10.1063/1.1614854.
Hofmann, B.A., Lorenzetti, S., Eugster, O., Krähenbühl, U., Herzog, G., Gnos, E., Eggimann, M., Wasson, J.T., 2009. The Twannberg (Switzerland) IIG iron meteorites: mineralogy, chemistry and CRE ages. Meteoritics Planet. Sci. 44, 187–199. https://doi.org/10.1111/j.1945-5100.2009.tb00727.x.
Ischer, T., 1911. Die Erforschungsgeschichte der Pfahlbauten des Bielersees. Anzeiger für schweizerische Altertumskunde. Neue Folge 13, 65–81.
Jambon, A., 2017. Bronze Age iron: meteoritic or not? A chemical strategy. J. Archaeol. Sci. 88, 47–53. https://doi.org/10.1016/j.jas.2017.09.008.
Jambon, A., Doumet-Serhal, C., 2018. La Transition du fer météoritique au fer terrestre à Sidon (College Site). Archaeology and History in the Lebanon 48, 82–95.
Johnson, D., Tyldesley, J., Lowe, T., Withers, P.J., Grady, M.M., 2013. Analysis of a prehistoric Egyptian iron bead with implications for the use and perception of meteorite iron in ancient Egypt. Meteoritics Planet. Sci. 48, 997–1006. https://doi.org/10.1111/maps.12120.
Johnson, D., Tyldesley, J., 2016. Iron from the sky. The role of meteorite iron in the development of iron-working techniques in ancient Egypt. In: Tyldesley, J., Price, C., Forshaw, R., Chamberlain, A., Nicholson, P.T., Morkot, R. (Eds.), Mummies, Magic and Medicine in Ancient Egypt, 1 ed. Manchester University Press, pp. 408–423.
Kass, R.E., Raftery, A.E., 1995. Bayes factors. J. Am. Stat. Assoc. 90, 773–795. URL: http://www.jstor.org/stable/2291091.
Kaul, F., Vrarberg, J., 2017. Danish beads of Egyptian and Mesopotamian glass in context, and the amber connection. In: Bergerbrant, S., Wessman, A. (Eds.), New Perspectives on the Bronze Age. Archaeopress Archaeology, pp. 375–386. Oxford.
Kotowiecki, A., 2004. Artefacts in Polish collections made of meteoritic iron. Meteoritics Planet. Sci. 39, A151–A156. https://doi.org/10.1111/j.1945-5100.2004.tb00351.x.
Leya, I., Masarik, J., 2009. Cosmogenic nuclides in stony meteorites revisited. Meteoritics Planet. Sci. 44, 1061–1086. https://doi.org/10.1111/j.1945-5100.2009.tb00788.x.
Losiak, A., Wild, E.M., Geppert, W.D., Huber, M.S., Jõeleht, A., Kriiska, A., Kulkov, A., Paavel, K., Pirkovic, I., Plado, J., Steier, P., Välja, R., Wilk, J., Wisniowski, T., Zanetti, M., 2016. Dating a small impact crater: an age of Kaali crater (Estonia) based on charcoal emplaced within proximal ejecta. Meteoritics Planet. Sci. 51, 681–695. https://doi.org/10.1111/maps.12616.
Matsui, T., Moriwaki, R., Zidan, E., Arai, T., 2022. The manufacture and origin of the Tutankhamen meteoritic iron dagger. Meteoritics Planet. Sci. 57, 747–758. https://doi.org/10.1111/maps.13787.
McCoy, T.J., Marquardt, A.E., Wasson, J.T., Ash, R.D., Vicenzi, E.P., 2017. The Anoka, Minnesota iron meteorite as parent to Hopewell meteoritic metal beads from Havana, Illinois. J. Archaeol. Sci. 81, 13–22. https://doi.org/10.1016/j.jas.2017.03.003.
Piaskowski, J., 1982. A study of the origin of the ancient high Ni iron generally regarded as meteoritic. In: Wertime, T.A., Wertime, S.F. (Eds.), Early Pyrotechnology. Smithsonian Institution, Washington DC, pp. 237–243.
Plado, J., 2012. Meteorite impact craters and possibly impact-related structures in Estonia. Meteoritics Planet. Sci. 47, 1590–1605. https://doi.org/10.1111/j.1945-5100.2012.01422.x.
Plado, J., 2021. Personal communication. November 5, 2021.
Ramírez García, D., Baur, D., Grigat, J., Hofmann, B.A., Lindemann, S., Masson, D., Schumann, M., von Sivers, M., Toschi, F., 2022. GeMSE: a low-background facility for gamma-spectrometry at moderate rock overburden. J. Instrum. 17, P04005 https://doi.org/10.1088/1748-0221/17/04/p04005.
Rasmussen, K.L., Aaby, B., Gwozdz, R., 2000. The age of the Kaalijärv meteorite craters. Meteoritics Planet. Sci. 35, 1067–1071. https://doi.org/10.1111/j.1945-5100.2000.tb01493.x.
Raukas, A., 2000. Investigation of impact spherules - a new promising method for the correlation of Quaternary deposits. Quat. Int. 68–71, 241–252. https://doi.org/10.1016/S1040-6182(00)00047-1.
Rehren, T., Belgya, T., Jambon, A., Káli, G., Kasztovszky, Z., Kis, Z., Kovács, I., Maróti, B., Martinón-Torres, M., Miniaci, G., Pigott, V.C., Radivojevi, M., Rosta, L., Szentmiklósi, L., Szökefalvi-Nagy, Z., 2013. 5,000 years old Egyptian iron beads made from hammered meteoritic iron. J. Archaeol. Sci. 40, 4785–4792. https://doi.org/10.1016/j.jas.2013.06.002.
Rickard, T.A., 1941. The use of meteoric iron. J. Roy. Anthropol. Inst. G. B. Ireland 71, 55–66. https://doi.org/10.2307/2844401.
Rosén, Å.V., Hofmann, B.A., Preusser, F., Gnos, E., Eggenberger, U., Schumann, M., Szidat, S., 2021. Meteorite terrestrial ages in Oman based on gamma spectrometry and sediment dating, focusing on the Ramlat Fasad dense collection area. Meteoritics Planet. Sci. 56, 2017–2034. https://doi.org/10.1111/maps.13758.
Rosén, Å.V., Hofmann, B.A., Sivers, M., Schumann, M., 2019. Radionuclide activities in recent chondrite falls determined by gamma-ray spectrometry: implications for terrestrial age estimates. Meteoritics Planet. Sci. 55, 149–163. https://doi.org/10.1111/maps.13427.
Saarse, L., Rajamäe, R., Heinsalu, A., Vassiljev, J., 1991. The biostratigraphy of sediments deposited in the Lake Kaali meteorite impact structure, Saaremaa island, Estonia. Bull. Geol. Soc. Finland 63, 129–139.
Scott, E.R.D., Wasson, J.T., 1976. Chemical classification of iron meteorites - VIII. Groups IC, IIE, IIIF and 97 other irons. Geochim. Cosmochim. Acta 40, 103–115. https://doi.org/10.1016/0016-7037(76)90198-8.
Scott, E.R.D., 2020. Iron Meteorites: Composition, Age, and Origin. Oxford University Press, Oxford. https://doi.org/10.1093/acrefore/9780190647926.013.206.
Shramko, B.A., 1981. Die ältesten Eisenfundstücke in Osteuropa (the oldest iron finds in eastern Europe). In: Haefner, H. (Ed.), Frühes Eisen in Europa. Meili, pp. 109–114. Schaffhausen (Switzerland).
Shramko, B.A., Fomin, L.D., Solntsev, L.A., 1965. ПЕРВАЯ НАХОДКА ИЗДЕЛИЯ ИЗ МЕТЕОРИТНОГО ЖЕЛЕЗА В ВОСТОЧНОЙ ЕВРОПЕ (The first find of a meteoritic iron product in eastern Europe). Sovjetskaja Archeologia 4, 199–204.
Smith, T., Hofmann, B.A., Leya, I., Merchel, S., Pavetich, S., Rugel, G., Scharf, A., 2017. The cosmic-ray exposure history of the Twannberg iron meteorite (IIG). Meteoritics Planet. Sci. 52, 2241–2257. https://doi.org/10.1111/maps.12928.
Smith, T., Cook, D.L., Merchel, S., Pavetich, S., Rugel, G., Scharf, A., Leya, I., 2019. The constancy of galactic cosmic rays as recorded by cosmogenic nuclides in iron meteorites. Meteoritics Planet. Sci. 54, 2951–2976. https://doi.org/10.1111/maps.13417.
Stankowski, W.T.J., 2001. The geology and morphology of the natural reserve "Meteoryt Morasko". Planet. Space Sci. 49, 749–753. https://doi.org/10.1016/S0032-0633(01)00011-3.
Ströbele, F., Broschat, K., Köberl, C., Zipfel, J., Hassan, H., Eckmann, C., 2016. The iron objects of Tutankhamun. METALLA Sonderheft 8 - Archäometrie und Denkmalpflege 2016 186–189.
Szokaluk, M., Jagodziński, R., Muszyński, A., Szczuciński, W., 2019. Geology of the Morasko craters, Poznan, Poland: small impact craters in unconsolidated sediments. Meteoritics Planet. Sci. 54, 1478–1494. https://doi.org/10.1111/maps.13290.
Tamm, K., 2014. Kaali Meteoriidi Voimalik Kasutamine Saaremaa Sepikodades (Possible Usage of Kaali Meteorite in Smitheries of Saaremaa). Master thesis. Institute of Geology, University of Tartu, p. 26. http://hdl.handle.net/10062/41566.
Terada, K., Ninomiya, K., Osawa, T., Tachibana, S., Miyake, Y., Kubo, M.K., Kawamura, N., Higemoto, W., Tsuchiyama, A., Ebihara, M., Uesugi, M., 2014. A new x-ray fluorescence spectroscopy for extraterrestrial materials using a muon beam. Sci. Rep. 4, 5072. https://doi.org/10.1038/srep05072.
Terada, K., Sato, A., Ninomiya, K., Kawashima, Y., Shimomura, K., Yoshida, G., Kawai, Y., Osawa, T., Tachibana, S., 2017. Non-destructive elemental analysis of a carbonaceous chondrite with direct current muon beam at music. Sci. Rep. 7, 15478 https://doi.org/10.1038/s41598-017-15719-5.
Trabska, J., Weselucha-Birczynska, A., Zieba-Palus, J., Runge, M.T., 2011. Black painted pottery, kildehuse II, odense county, Denmark. Spectrochim. Acta Mol. Biomol. Spectrosc. 79, 824–830.
Tschumi, O., 1953. Urgeschichte des Kantons Bern. Hans Huber, Bern and Stuttgart.
von Fellenberg, E., 1875. Bericht an die Tit. Direktion der Entsumpfungen über die Ausbeutung der Pfahlbauten des Bielersees im Jahre 1873 und 1874. Mitteilung der Naturforschenden Gesellschaft Bern für das Jahr 1874, 263–358.
von Sivers, M., Hofmann, B., Rosén, Å., Schumann, M., 2016. The GeMSE facility for low-background γ-ray spectrometry. J. Instrum. 11, P12017 https://doi.org/10.1088/1748-0221/11/12/p12017. – P12017.
Veski, S., Heinsalu, A., Kirsimäe, K., Poska, A., Saarse, L., 2001. Ecological catastrophe in connection with the impact of the Kaali Meteorite about 800-400 BC on the island of Saaremaa, Estonia. Meteoritics Planet. Sci. 36, 1367–1376. https://doi.org/10.1111/j.1945-5100.2001.tb01830.x.
Veski, S., Heinsalu, A., Lang, V., Kestlane, Ü.l., Possnert, G., 2004. The age of the Kaali meteorite craters and the effect of the impact on the environment and man: evidence from inside the Kaali craters, island of Saaremaa, Estonia. Veg. Hist. Archaeobotany 13, 197–206. https://doi.org/10.1007/s00334-004-0043-x.
Wasson, J.T., Kallemeyn, G.W., 2002. The IAB iron-meteorite complex: a group, five subgroups, numerous grouplets, closely related, mainly formed by crystal segregation in rapidly cooling melts. Geochim. Cosmochim. Acta 66, 2445–2473. https://doi.org/10.1016/S0016-7037(02)00848-7.
Wasson, J.T., Choe, W.-H., 2009. The IIG iron meteorites: probable formation in the IIAB core. Geochim. Cosmochim. Acta 73, 4879–4890. https://doi.org/10.1016/j.gca.2009.05.062.
Wasson, J.T., Huber, H.J., Malvin, D.J., 2007. Formation of IIAB iron meteorites. Geochim. Cosmochim. Acta 71, 760–781. https://doi.org/10.1016/S0016-7037(02)00848-7.
Wesel, R., 2004-2019. Kaali, Kaalijärv. http://www.nakhladogmeteorites.com/catalog/kaali.htm.
Zavyalov, V.I., Terekhova, N.N., 2019. Meteoritic iron artefacts redux. Archeol. Rozhl. 71, 155–167. https://www.arup.cas.cz/wp-content/uploads/2021/11/1.Zavyalov-Terekhova_155-167.pdf.